

## RESEARCH ARTICLE

View Article Online  
View Journal | View IssueCite this: *Inorg. Chem. Front.*, 2025, 12, 1950

# Ca<sub>2</sub>La(MS<sub>4</sub>)(BS<sub>3</sub>) (M = Ge/Si and Sn/Si): high-performance infrared nonlinear optical materials designed using an atomic site co-occupancy strategy†

Ya-Xiang Han,<sup>a,b</sup> Chun-Li Hu<sup>a</sup> and Jiang-Gao Mao \*<sup>a</sup>

Exploration of new material systems and optical performance enhancement are huge challenges for the study of infrared nonlinear optical (IR NLO) materials. In this work, the first thioborate-thiogermanate and thioborate-thiostannate compounds, Ca<sub>2</sub>La(Ge<sub>0.72</sub>Si<sub>0.28</sub>S<sub>4</sub>)(BS<sub>3</sub>) and Ca<sub>2</sub>La(Sn<sub>0.75</sub>Si<sub>0.25</sub>S<sub>4</sub>)(BS<sub>3</sub>), containing both co-occupied Ca<sup>2+</sup>/La<sup>3+</sup> cation and [Ge/SiS<sub>4</sub>]<sup>4-</sup> or [Sn/SiS<sub>4</sub>]<sup>4-</sup> anion sites, respectively, were designed through an atomic site co-occupancy strategy. They inherited favourable 3D network structures in which the effectively aligned [MS<sub>4</sub>]<sup>4-</sup> and [BS<sub>3</sub>]<sup>3-</sup> functional anions were bridged by Ca<sup>2+</sup>/La<sup>3+</sup> cations. Remarkably, the title compounds achieved excellent IR NLO properties, including good chemical and thermal stabilities, wide light transmission ranges (0.45–11 μm), strong second harmonic generation responses (1.5 and 2.0 times that of commercial AgGaS<sub>2</sub> at 2.05 μm) and high laser-induced damage thresholds (7 and 6 times that of AgGaS<sub>2</sub>). Theoretical calculation and experimental results revealed that, on the basis of excellent structural framework, introducing more active functional groups through atomic site co-occupancy could simultaneously enhance the second harmonic generation effect and maintain a relatively high laser-induced damage threshold. This work not only offers an easier synthetic route for mixed anionic thioborates but also provides inspiration for the design of well-performed NLO materials.

Received 29th November 2024,  
Accepted 6th January 2025

DOI: 10.1039/d4qi03060e

rsc.li/frontiers-inorganic

## Introduction

There are urgent demands for infrared nonlinear optical crystals with various advanced optical applications, such as optical communication, optical imaging, laser guidance and so on.<sup>1–4</sup> However, the commercially available IR NLO crystals suffer from many drawbacks, such as the low laser-induced damage threshold (LIDT) of AgGaS<sub>2</sub>, the poor phase matching ability of AgGaSe<sub>2</sub>, and the detrimental two-photon absorption of ZnGeP<sub>2</sub>.<sup>5–7</sup> Meanwhile, the conflict between large NLO coefficient and wide band gap hinders the achievement of overall excellent properties. Hence, the explorations of novel high-performance IR NLO materials with large nonlinear coefficients, phase matching ability (appropriate Δ*n*), high laser-induced

damage threshold (LIDT), wide optical transmission range, and high physical and chemical stability remain a hot topic.<sup>8–10</sup>

To achieve unique non-centrosymmetric structures and improved IR NLO performance, increasing the diversity of components in chalcogenides has become a mainstream method.<sup>11–16</sup> Starting from the typical chalcopyrite configuration, numerous diamond-like IR NLO materials composed of different tetrahedral motifs have been explored, such as Hg<sub>3</sub>P<sub>2</sub>S<sub>8</sub> (4.2 × AGS) and Li<sub>2</sub>ZnSi<sub>4</sub> (1.2 × AGS).<sup>17–20</sup> In addition, cations with different coordination geometries have been combined with tetrahedral units, which led to the discovery of materials such as 3D close-packed Eu<sub>2</sub>P<sub>2</sub>S<sub>6</sub>, 3D tunnel structural Li<sub>4</sub>MgGe<sub>2</sub>S<sub>7</sub> (0.7 × AGS), 2D layered SrZnGeS<sub>4</sub> (0.9 × AGS) or salt-inclusion [ABa<sub>2</sub>Cl][Ga<sub>4</sub>S<sub>8</sub>] (A = Rb, Cs; 0.9 and 1 × AGS).<sup>21–28</sup> Besides the mainstream tetrahedral motifs, planar triangular groups, which exhibit large hyperpolarizabilities and polarizability anisotropies, have also caught researchers' eye.<sup>29–31</sup> Among them, the π-conjugated BS<sub>3</sub> trigonal planar unit can not only produce strong second harmonic generation (SHG) response and large birefringence but simultaneously facilitate high LIDT, as exemplified by BaB<sub>2</sub>S<sub>4</sub> (0.8 × AGS) and LaBS<sub>3</sub> (1.2 × AGS).<sup>32–35</sup> However, due to the immature synthesis method and worrying stability of thioborates, there are still

<sup>a</sup>State Key Laboratory of Structural Chemistry, Fujian Institute of Research on the Structure of Matter, Chinese Academy of Sciences, Fuzhou, 350002, P. R. China.  
E-mail: mjg@fjirsm.ac.cn

<sup>b</sup>University of Chinese Academy of Sciences, Beijing 100039, P. R. China

†Electronic supplementary information (ESI) available: Syntheses, methods, instrumentations, computational details, crystallographic data, LIDT test results, powder XRD, thermal analysis and computational results of title compounds. CCDC 2386136 and 2386137. For ESI and crystallographic data in CIF or other electronic format see DOI: <https://doi.org/10.1039/d4qi03060e>

few IR NLO materials containing  $\text{BS}_3$  groups up to now.<sup>36</sup> Committed to exploring new material systems, the first thioborate–thiosilicates,  $\text{Ca}_2\text{Ln}(\text{BS}_3)(\text{SiS}_4)$  (Ln = La, Ce, and Gd;  $\approx 1 \times \text{AGS}$ ), containing both triangular  $\text{BS}_3$  and tetrahedral  $\text{SiS}_4$  units have been recently reported by our group.<sup>37</sup>

Introducing defects or disorders has been demonstrated to be able to adjust the polarizations, alignments, and densities of functional groups.<sup>38</sup> For instance, in  $\text{Pb}_{2.15}\text{Li}_{0.85}\text{Nb}_{4.85}\text{Ti}_{0.15}\text{O}_{15}$  and  $\text{Pb}_{2.15}\text{Li}_{0.55}\text{Nb}_{4.85}\text{W}_{0.15}\text{O}_{15}$ , doping transition metal  $\text{Ti}^{4+}$  or  $\text{W}^{6+}$  cations into the  $\text{Nb}^{5+}$  sites increased the distortion of the  $\text{Nb}/\text{MO}_6$  octahedra, producing a significantly enhanced SHG effect ( $56$  and  $67 \times \text{KH}_2\text{PO}_4$ ).<sup>39</sup> Additionally, the vacancies in  $\text{Pb}_{1.91}\text{K}_{3.22}\square_{0.85}\text{Li}_{2.96}\text{Nb}_{10}\text{O}_{30}$  ( $\square$ : vacancies) also contributed to its notable SHG effect ( $\approx 71.5 \times \text{KH}_2\text{PO}_4$ ).<sup>40</sup> Similar examples have also been found in IR NLO materials.<sup>41,42</sup> After doping the  $\text{Na}^+$  sites with  $\text{Ag}^+$  or doping  $\text{Ag}^+$  positions with  $\text{Li}^+$ ,  $\text{Na}_2\text{Ba}[(\text{Ag}_{0.9}\text{Na}_{0.1})_2\text{Sn}_2\text{S}_7]$  and  $\text{LiAgIn}_2\text{GeS}_6$  achieved a stronger SHG effect ( $1.6$  and  $0.8 \times \text{AGS}$ , respectively).<sup>43,44</sup> However, these cases are based on the cation introduction, which led to weak performance changes.

Inspired by the above results, and considering the benefits of the structure frame on optical anisotropy ( $\Delta n = 0.149$ ) and large laser damage threshold ( $10 \times \text{AGS}$ ) in  $\text{Ca}_2\text{La}(\text{BS}_3)(\text{SiS}_4)$ , we aim to dope more flexible  $\text{Ge}^{4+}$  and  $\text{Sn}^{4+}$  into the  $\text{Si}^{4+}$  site in  $\text{Ca}_2\text{Ln}(\text{BS}_3)(\text{SiS}_4)$  to further enhance the IR NLO performances.<sup>34</sup> As a result, the first examples of thioborate–thiogermanates and thioborate–thiostannates, namely,  $\text{Ca}_2\text{La}(\text{Ge}_{0.72}\text{Si}_{0.28}\text{S}_4)(\text{BS}_3)$  and  $\text{Ca}_2\text{La}(\text{Sn}_{0.75}\text{Si}_{0.25}\text{S}_4)(\text{BS}_3)$ , have been successfully designed and synthesized. They crystallize in the polar space group  $P6_3mc$ , featuring a 3D network structure in which the discrete  $[\text{BS}_3]^{3-}$  and  $[\text{MS}_4]^{4-}$  ( $\text{M} = \text{Ge}/\text{Si}$  and  $\text{Sn}/\text{Si}$ ) anionic groups are interconnected by the co-occupied  $\text{Ca}^{2+}$  and  $\text{La}^{3+}$  cations. In addition, they exhibit stronger SHG effects ( $1.5$  and  $2.0$  times that of commercial AGS), good chemical and thermal stabilities, wide light transmission range ( $0.45$ – $11 \mu\text{m}$ ) and high laser-induced damage thresholds ( $7$  and  $6$  times that of AGS), which prove that  $\text{Ca}_2\text{La}(\text{MS}_4)(\text{BS}_3)$  ( $\text{M} = \text{Ge}/\text{Si}$  and  $\text{Sn}/\text{Si}$ ) are promising infrared nonlinear optical materials.

## Results and discussion

### Syntheses

The single crystals of  $\text{Ca}_2\text{La}(\text{MS}_4)(\text{BS}_3)$  ( $\text{M} = \text{Ge}/\text{Si}$  and  $\text{Sn}/\text{Si}$ ) were synthesized by solid-state reactions in sealed  $\text{SiO}_2$  tubes at  $900$  and  $950 \text{ }^\circ\text{C}$  with  $\text{BaS}$ ,  $\text{CaS}$ ,  $\text{La}_2\text{S}_3$ ,  $\text{GeO}_2$  (or  $\text{SnO}_2$ ),  $\text{B}$  and  $\text{S}$  powders as reactants (ESI†). During our previous syntheses of  $\text{Ca}_2\text{Ln}(\text{SiS}_4)(\text{BS}_3)$  (Ln = La, Ce, and Gd), the replacement reaction between  $\text{B}$  ( $\text{B}_2\text{S}_3$ ) and  $\text{SiO}_2$  was utilized to form the Si–B–S system.<sup>45</sup> The successful syntheses of  $\text{Ca}_2\text{La}(\text{MS}_4)(\text{BS}_3)$  proved that this method can be extended to other group 14 element–B–S systems, which is of great significance in overcoming the synthetic difficulties of thioborates caused by the strong affinity of boron to oxygen. It is worth mentioning that similar reactions were also previously used by Guo *et al.* for the synthesis of thiosilates and thiogermanates.<sup>46,47</sup>

### Phase analysis

The purities of  $\text{Ca}_2\text{La}(\text{MS}_4)(\text{BS}_3)$  ( $\text{M} = \text{Ge}/\text{Si}$  and  $\text{Sn}/\text{Si}$ ) were validated by the powder X-ray diffraction studies (Fig. 1a and b). Energy-dispersive X-ray spectroscopy (EDS) analyses revealed the presence of Ca, La, M and S atoms (Fig. 1c and d) with molar ratios  $1.8 : 1 : 0.7 : 0.3 : 5.5$  and  $1.8 : 1 : 0.8 : 0.2 : 6.7$  for  $\text{Ca}_2\text{La}(\text{Ge}_{0.72}\text{Si}_{0.28}\text{S}_4)(\text{BS}_3)$  and  $\text{Ca}_2\text{La}(\text{Sn}_{0.75}\text{Si}_{0.25}\text{S}_4)(\text{BS}_3)$ , respectively, which are very close to the results of the X-ray structural analysis. The presence of the B element is confirmed by the presence of the infrared absorption bands associated with the  $[\text{BS}_3]^{3-}$  unit in the IR spectra.

### Crystal structure

$\text{Ca}_2\text{La}(\text{MS}_4)(\text{BS}_3)$  ( $\text{M} = \text{Ge}/\text{Si}$  and  $\text{Sn}/\text{Si}$ ) are isostructural and crystallize in the hexagonal polar space group  $P6_3mc$  (No. 186). They are also isostructural to  $\text{Ca}_2\text{Ln}(\text{BS}_3)(\text{SiS}_4)$ , but exhibit lattice distortion, which can be proved by the overall small-angle shift of their PXRD peaks (Fig. S1†).<sup>34</sup> The asymmetric unit of  $\text{Ca}_2\text{La}(\text{MS}_4)(\text{BS}_3)$  ( $\text{M} = \text{Ge}/\text{Si}$  and  $\text{Sn}/\text{Si}$ ) is composed of one mixed site of  $\text{Ca}^{2+}$  and  $\text{La}^{3+}$ , one mixed site of  $\text{Si}^{4+}$  and  $\text{Ge}^{4+}$  or  $\text{Sn}^{4+}$ , one B, and three S atoms. In  $\text{Ca}_2\text{La}(\text{Ge}_{0.72}\text{Si}_{0.28}\text{S}_4)(\text{BS}_3)$ , the refined occupancy factors of  $\text{Ca}^{2+}$  and  $\text{La}^{3+}$  are  $0.652(3)$  and  $0.348(3)$ , respectively, and those of  $\text{Ge}^{4+}$  and  $\text{Si}^{4+}$  are  $0.720(8)$  and  $0.280(8)$ , respectively. In  $\text{Ca}_2\text{La}(\text{Sn}_{0.75}\text{Si}_{0.25}\text{S}_4)(\text{BS}_3)$ , the refined occupancy factors of  $\text{Ca}^{2+}$  and  $\text{La}^{3+}$  are  $0.619(3)$  and  $0.381(3)$ , respectively, and those of  $\text{Sn}^{4+}$  and  $\text{Si}^{4+}$  are  $0.755(9)$  and  $0.245(9)$ , respectively (Tables S1 and S2, ESI†). The Ca(1)/La(1), S(2) and S(3) atoms lie on the 6c site, whereas Ge(1)/Si(1), B(1) and S(1) occupy the 2a sites. As shown in Fig. 2a and Fig. S2a,† the structure of  $\text{Ca}_2\text{La}(\text{MS}_4)(\text{BS}_3)$  can be also viewed as a derivative of  $\text{Sr}_3[\text{SnOSe}_3][\text{CO}_3]$  where Sr,  $\text{SnOSe}_3$ , and  $\text{CO}_3$  units are substituted by Ca/La,  $\text{MS}_4$ ,  $\text{BS}_3$  groups, respectively.<sup>48</sup> Both compounds feature a three-dimensional network composed of discrete tetrahedral and planar triangular anions interconnected by counter-metal cations (Fig. 2b and Fig. S2b†). Differently, in the  $\text{Ca}_2\text{La}(\text{MS}_4)(\text{BS}_3)$ , the  $[\text{BS}_3]^{3-}$  triangles and  $\text{MS}_4$  tetrahedra are arranged perfectly parallel to the ac plane, creating a sixfold rotation symmetry. While in  $\text{Sr}_3[\text{SnOSe}_3][\text{CO}_3]$  with a lower symmetric  $Pmn2_1$  space group, the  $\text{CO}_3$  and  $\text{SnOSe}_4$  groups are not well aligned. The aligned active groups in  $\text{Ca}_2\text{La}(\text{MS}_4)(\text{BS}_3)$  are advantageous for nonlinear optical crystals, which facilitates the efficient superposition of the microscopic nonlinear coefficients, contributing to a stronger macroscopic SHG effect ( $1.5$  and  $2.0 \times \text{AGS}$ ) than that by  $\text{Sr}_3[\text{SnOSe}_3][\text{CO}_3]$  ( $1.0 \times \text{AGS}$ ).

### Thermal analysis

As shown in Fig. S3,† thermogravimetric analysis (TGA) and differential thermal analysis (DTA) curves measured under the  $\text{N}_2$  atmosphere revealed that the  $\text{Ca}_2\text{La}(\text{Ge}_{0.72}\text{Si}_{0.28}\text{S}_4)(\text{BS}_3)$  and  $\text{Ca}_2\text{La}(\text{Sn}_{0.75}\text{Si}_{0.25}\text{S}_4)(\text{BS}_3)$  are stable up to about  $700 \text{ }^\circ\text{C}$ , which are lower stabilities than that of  $\text{Ca}_2\text{Ln}(\text{BS}_3)(\text{SiS}_4)$  ( $880 \text{ }^\circ\text{C}$ ).<sup>34</sup> This may be due to the weaker M–S covalent bonds compared to the Si–S bonds.

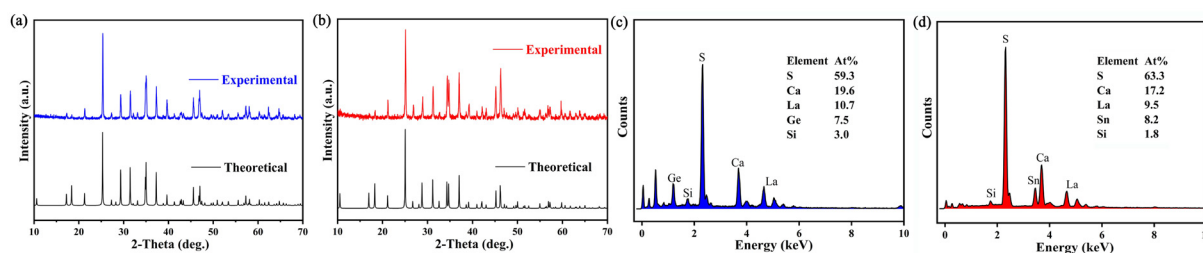


Fig. 1 Powder X-ray diffraction patterns and EDS maps for  $\text{Ca}_2\text{La}(\text{Ge}_{0.72}\text{Si}_{0.28}\text{S}_4)(\text{BS}_3)$  (a and c) and  $\text{Ca}_2\text{La}(\text{Sn}_{0.75}\text{Si}_{0.25}\text{S}_4)(\text{BS}_3)$  (b and d).

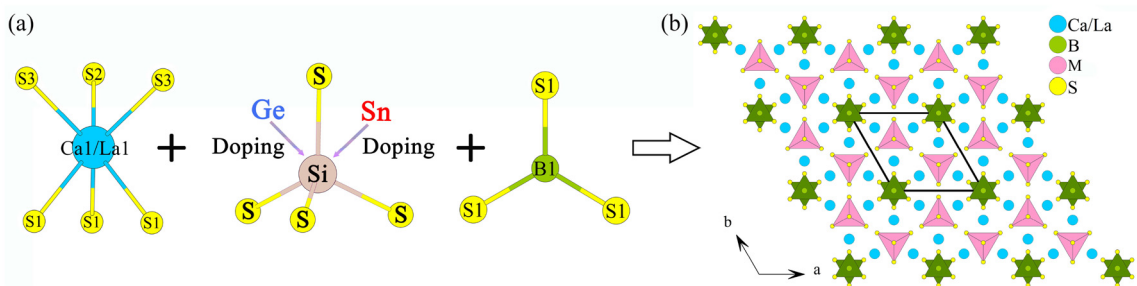


Fig. 2  $\text{CaS}_6$ ,  $\text{MS}_4$  and  $\text{BS}_3$  functional motifs in  $\text{Ca}_2\text{La}(\text{MS}_4)(\text{BS}_3)$  ( $M = \text{Ge/Si}$  and  $\text{Sn/Si}$ ) (a), and the overall crystal structure of  $\text{Ca}_2\text{La}(\text{MS}_4)(\text{BS}_3)$  viewed down the  $c$ -axis (b).

## Optical properties

Raman spectra of both compounds exhibit no absorption peaks in the range of 500 to 4000  $\text{cm}^{-1}$  (Fig. 3a). The characteristic peaks at 366, 388, 445  $\text{cm}^{-1}$  for  $\text{Ca}_2\text{La}(\text{Ge}_{0.72}\text{Si}_{0.28}\text{S}_4)(\text{BS}_3)$  and 350, 422, 442  $\text{cm}^{-1}$  for  $\text{Ca}_2\text{La}(\text{Sn}_{0.75}\text{Si}_{0.25}\text{S}_4)(\text{BS}_3)$  are associated with vibrations of Ge-S and Sn-S bond, respectively, which are in good agreement with the reported data of  $\text{Na}_2\text{Hg}_3\text{M}_2\text{S}_8$ .<sup>49</sup> In addition, the characteristic peaks at low energy area (120, 146, 150 and 225  $\text{cm}^{-1}$ ) can be assigned to Ca/La-S bonds referring to  $\text{La}_3\text{LiMS}_7$ .<sup>50</sup>

As shown in the IR spectra (Fig. 3b),  $\text{Ca}_2\text{La}(\text{MS}_4)(\text{BS}_3)$  ( $M = \text{Ge/Si}$  and  $\text{Sn/Si}$ ) show good light transmission in the 4000–900  $\text{cm}^{-1}$  range. Since the IR absorption bands are dominated by the  $[\text{BS}_3]^{3-}$  and  $[\text{SiS}_4]^{4-}$  groups, their IR spectra are very similar. The absorption bands at  $\approx 800$ –900  $\text{cm}^{-1}$  and

400  $\text{cm}^{-1}$  can be attributed to the asymmetrical B-S stretching E modes and symmetrical B-S stretching A<sub>1</sub> modes of the  $(\text{BS}_3)^{3-}$  units, respectively.<sup>51</sup> In addition, the strong absorption peak at  $\approx 500$   $\text{cm}^{-1}$  can be attributed to Si-S bond vibrations.

UV-vis-NIR diffuse reflectance spectra revealed the band gaps of 3.15 and 2.62 eV for  $\text{Ca}_2\text{La}(\text{Ge}_{0.72}\text{Si}_{0.28}\text{S}_4)(\text{BS}_3)$  and  $\text{Ca}_2\text{La}(\text{Sn}_{0.75}\text{Si}_{0.25}\text{S}_4)(\text{BS}_3)$ , respectively (Fig. 3c), which matches with their pale yellow and yellow colours. It is worth mentioning that their band gaps are close to those of  $\text{LaLi}_3\text{GeS}_7$  (3.02 eV) and  $\text{LaLi}_3\text{SnS}_7$  (2.40 eV), which indicate that their obviously different band gaps are mainly determined by the  $\text{GeS}_4$  and  $\text{SnS}_4$  groups.<sup>50</sup> Combining the IR spectra,  $\text{Ca}_2\text{La}(\text{MS}_4)(\text{BS}_3)$  ( $M = \text{Ge/Si}$  and  $\text{Sn/Si}$ ) show good light transmittance in the visible to mid-IR spectrum range of 0.45–11  $\mu\text{m}$ , suggesting their potential as IR NLO materials.

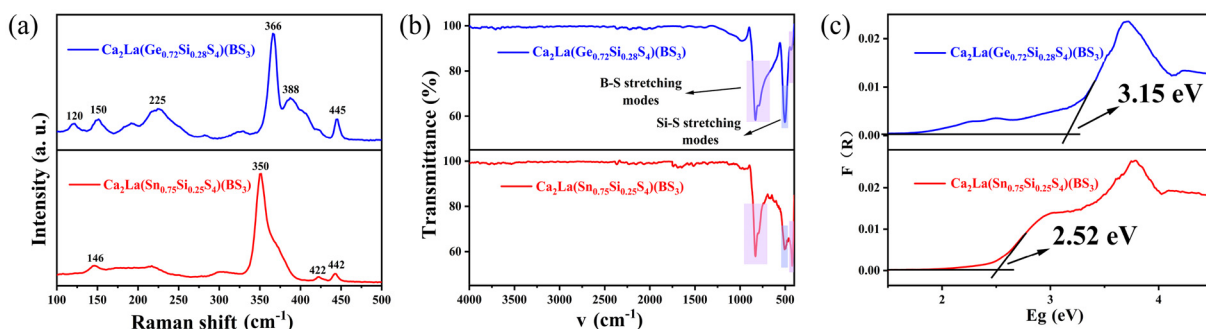


Fig. 3 Raman spectra (a), Fourier transform infrared spectra (b) and UV-vis-IR diffuse reflectance spectra (c) of the title compounds.

## SHG and LIDT performances

Powder SHG measurements indicate that both  $\text{Ca}_2\text{La}(\text{Ge}_{0.72}\text{Si}_{0.28}\text{S}_4)(\text{BS}_3)$  and  $\text{Ca}_2\text{La}(\text{Sn}_{0.75}\text{Si}_{0.25}\text{S}_4)(\text{BS}_3)$  exhibit strong SHG effects, which are 1.5 and 2.0 times that of commercial AGS at 2.05  $\mu\text{m}$ , respectively (Fig. 4a). Additionally, particle size-dependent SHG curves suggest that they are type-I phase-matchable (Fig. 4b). Compared to  $\text{Ca}_2\text{La}(\text{SiS}_4)(\text{BS}_3)$  ( $1.0 \times \text{AGS}$ ),  $\text{Ca}_2\text{La}(\text{MS}_4)(\text{BS}_3)$  achieved significant SHG enhancement, which may be attributed to the introduction of  $\text{GeS}_4$  and  $\text{SnS}_4$  functional motifs with larger polarization abilities and higher SHG activities. To directly prove this, the hyperpolarizabilities, which are generally considered to be positively correlated with SHG activity, of standard  $\text{SiS}_4$ ,  $\text{GeS}_4$  and  $\text{SnS}_4$  units were calculated to be 67, 103 and 111, respectively, by using LANL2DZ base group in the Gaussian 09 program based on a semi-empirical method.<sup>52</sup> The same trends of experimental and calculated results justify the atomic site co-occupancy strategy of introducing  $\text{GeS}_4$  and  $\text{SnS}_4$  groups to enhance the SHG effect.

Laser-induced damage threshold tests were performed by radiating the microcrystalline particles with 1 HZ 1064 nm laser. The LIDT values of  $\text{Ca}_2\text{La}(\text{Ge}_{0.72}\text{Si}_{0.28}\text{S}_4)(\text{BS}_3)$  and  $\text{Ca}_2\text{La}(\text{Sn}_{0.75}\text{Si}_{0.25}\text{S}_4)(\text{BS}_3)$  were 26.36 and 25.37  $\text{MW cm}^{-2}$ , which are about 7 and 6 times that of AGS (4  $\text{MW cm}^{-2}$ ) (Table S4†). To further explain their higher LIDTs, the temperature-dependent cell parameters of both compounds were measured from 100 to 400 K (Fig. S4†). Linear fitting analysis showed that their thermal expansion coefficients (TEC) in the  $a$  ( $b$ ) axis and  $c$  axis are  $1.09 \times 10^{-5}$ ,  $1.25 \times 10^{-5} \text{ T}^{-1}$  and  $1.03 \times 10^{-5}$ ,  $1.38 \times 10^{-5} \text{ T}^{-1}$ , respectively, which are much smaller than that of AGS ( $2.09 \times 10^{-5}$ ,  $-1.07 \times 10^{-5} \text{ T}^{-1}$ ). In addition, the much smaller TEC anisotropy (0.15 and 0.34 to 2.95) also gives the explanation of their higher LIDTs (Table 1). Compared with  $\text{Ca}_2\text{La}(\text{SiS}_4)(\text{BS}_3)$ , the smaller LIDTs of title compounds are due to weaker covalent Ge/Sn-S bonds. However, the almost equally small TEC parameters indicate that the excellent crystal framework is the basis for them to achieve large polished damage thresholds. Furthermore, the SHG and LIDT performances comparison reveal that both  $\text{Ca}_2\text{La}(\text{MS}_4)(\text{BS}_3)$  exhibit obviously enhanced SHG effects among previously reported thioborates with considerable LIDTs.<sup>53</sup>

Table 1 TECs and TEAs of  $\text{Ca}_2\text{La}(\text{MS}_4)(\text{BS}_3)$  and AGS

| Compounds   | TEC ( $\times 10^{-5} \text{ T}^{-1}$ ) |       | TEA <sup>a</sup> |
|---|---|-------|------------------|
|   | $a$                                     | $c$   |                  |
| $\text{Ca}_2\text{La}(\text{Ge}_{0.72}\text{Si}_{0.28}\text{S}_4)(\text{BS}_3)$ | 1.09                                    | 1.25  | 0.15             |
| $\text{Ca}_2\text{La}(\text{Sn}_{0.75}\text{Si}_{0.25}\text{S}_4)(\text{BS}_3)$ | 1.03                                    | 1.38  | 0.34             |
| AGS   | 2.09                                    | -1.07 | 2.95             |

$$^a \text{TEA} = (\text{TEC}_{\text{max}} - \text{TEC}_{\text{min}}) / \text{TEC}_{\text{min}}$$

## Theoretical calculations

For further understanding of the relationship between structures and properties of title compounds, the first-principles calculations based on crystal structures and DFT methods were performed.<sup>54,55</sup> To facilitate the calculations, disorder-free structures of  $\text{Ca}_2\text{La}(\text{GeS}_4)(\text{BS}_3)$  and  $\text{Ca}_2\text{La}(\text{SnS}_4)(\text{BS}_3)$  were created by lowering the symmetry from the space group  $P6_3mc$  (No. 186) to  $Cmc2_1$  (No. 36), in which the six  $\text{Ln}_{1/3}\text{Ca}_{2/3}$  sites in the original cell were split into two Ln and four Ca atoms and the Ge/Si or Sn/Si sites were assigned as Ge or Sn, respectively. As shown in Fig. S5,† the indirect theoretical band gap values of  $\text{Ca}_2\text{La}(\text{GeS}_4)(\text{BS}_3)$  and  $\text{Ca}_2\text{La}(\text{SnS}_4)(\text{BS}_3)$  were calculated as 2.26 and 2.41 eV respectively, which are smaller compared to the experimental values due to the limitations of the GGA method. To calculate their optical properties more accurately, scissor operators of 0.89 and 0.11 eV were adopted during the subsequent optical property calculations.

The partial density of states (DOS) analysis (Fig. S6†) revealed that the band gap contributions of  $\text{Ca}_2\text{La}(\text{GeS}_4)(\text{BS}_3)$  and  $\text{Ca}_2\text{La}(\text{SnS}_4)(\text{BS}_3)$  are quite similar, which is due to their identical structures and similar chemical compositions. The topmost valence bands (VB) are dominated by the S-3p orbitals. The bottom of the conduction bands (CB), however, are contributed by La-5d, Ge-4s, Sn-5s and B-2p orbitals. Hence, the band gaps of the title compounds originate from the joint contribution of the  $\text{LaS}_6$ ,  $\text{MS}_4$ , and  $\text{BS}_3$  groups.

The theoretical birefringence values ( $\Delta n$ ) of  $\text{Ca}_2\text{La}(\text{GeS}_4)(\text{BS}_3)$  and  $\text{Ca}_2\text{La}(\text{SnS}_4)(\text{BS}_3)$  were calculated to be 0.141 and 0.155 at 1064 nm, respectively (Fig. S7†). The equal refractive index values of the fundamental and double frequency light

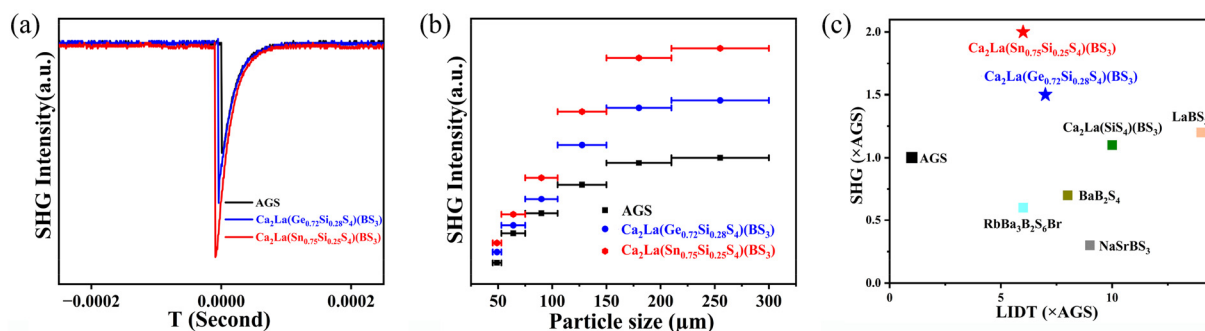


Fig. 4 Particle size-dependent SHG intensity curves for the title compounds (a) and (b); SHG and LIDT comparison of reported thioborates (c).

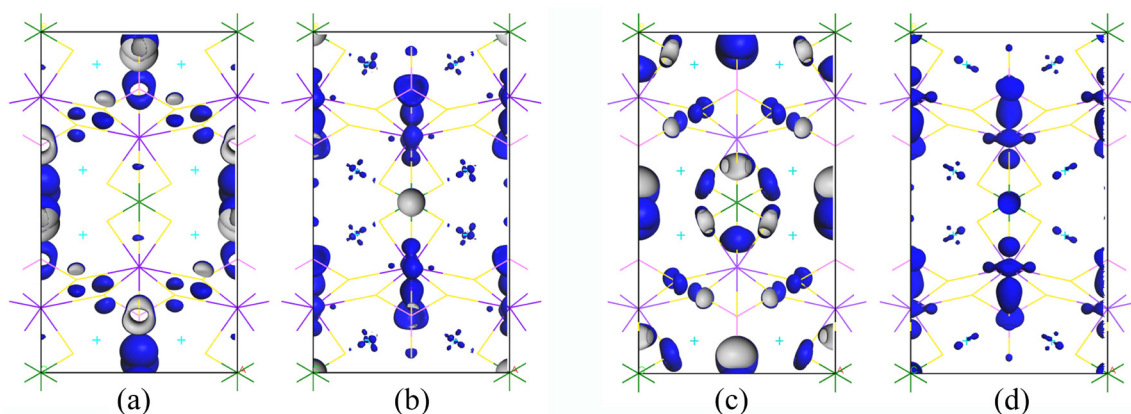


Fig. 5 SHG density plots for  $\text{Ca}_2\text{La}(\text{Ge}_{0.72}\text{Si}_{0.28}\text{S}_4)(\text{BS}_3)$  [VB (a) and CB (b)] and  $\text{Ca}_2\text{La}(\text{Sn}_{0.75}\text{Si}_{0.25}\text{S}_4)(\text{BS}_3)$  [VB (c) and CB (d)].

prove the phase matching ability of the title materials. Remarkably, the large  $\Delta n$  values of title compounds are close to those of  $\text{Sr}_3[\text{SnOSe}_3][\text{CO}_3]$  (0.16–0.13 at 400–700 nm) and  $\text{Ca}_2\text{La}(\text{SiS}_4)(\text{BS}_3)$  (0.149 at 1064 nm), indicating that combining anion groups with different geometries may be an effective way to achieve large birefringence.

Under the restriction of space group and Kleinman's symmetry, the largest independent SHG tensors of  $\text{Ca}_2\text{La}(\text{GeS}_4)(\text{BS}_3)$  and  $\text{Ca}_2\text{La}(\text{SnS}_4)(\text{BS}_3)$  were calculated to be  $d_{32} = 7.48$  and  $d_{33} = -15.61 \text{ pm V}^{-1}$ , respectively, which exhibit the same trend as the experimental results. Furthermore, the SHG-weighted electron density (SHG density) analyses for the largest independent SHG tensors were performed to reveal the distribution of the source of SHG effects. As shown in Fig. 5a and c, in the valence band, the SHG effects originate from S-3p (yellow) non-bonding states for both compounds; while in the conduction band (Fig. 5b and d), the SHG process is mainly dominated by the unoccupied La-5d (purple), Ge-4p or Sn-5p (pink) orbitals and B-S (green)  $\pi^*$  anti-bonding states, with few contributions from Ca-3d (blue) and S-3p orbitals. Furthermore, the SHG density over VB and CB was integrated to evaluate the contribution percentages of each structure-building group. For  $\text{Ca}_2\text{La}(\text{GeS}_4)(\text{BS}_3)$ , the SHG contribution percentages of  $\text{Ca}^{2+}$ ,  $\text{LaS}_6$ ,  $\text{GeS}_4$  and  $\text{BS}_3$  units are 3.8%, 29.66%, 49.34%, 17.10% respectively; for  $\text{Ca}_2\text{La}(\text{SnS}_4)(\text{BS}_3)$ , the SHG contribution percentages of  $\text{Ca}^{2+}$ ,  $\text{LaS}_6$ ,  $\text{SnS}_4$  and  $\text{BS}_3$  units are 3.3%, 29.59%, 43.75% and 47.18%, respectively. Hence, the strong SHG responses of  $\text{Ca}_2\text{La}(\text{MS}_4)(\text{BS}_3)$  mainly originate from the synergistic effects of three SHG-active  $\text{LaS}_6$ ,  $\text{MS}_4$  and  $\text{BS}_3$  groups.

## Conclusions

In summary, the first examples of thioborate-thiogermanates and thioborate-thiostannates, namely,  $\text{Ca}_2\text{La}(\text{Ge}_{0.72}\text{Si}_{0.28}\text{S}_4)(\text{BS}_3)$  and  $\text{Ca}_2\text{La}(\text{Sn}_{0.75}\text{Si}_{0.25}\text{S}_4)(\text{BS}_3)$ , were designed using an atomic site co-occupancy strategy. The syntheses of  $\text{Ca}_2\text{La}(\text{MS}_4)(\text{BS}_3)$  again support that the replacement reaction

between boron and oxide is helpful for the syntheses of mixed anionic thioborates. In addition,  $\text{Ca}_2\text{La}(\text{MS}_4)(\text{BS}_3)$  inherit a favourable crystal structure, in which both the  $\text{MS}_4$  tetrahedra and  $\text{BS}_3$  triangles are arranged parallel to the ac plane, facilitating an efficient superposition of the SHG effect. Furthermore, both materials achieved good chemical and thermal stabilities, wide transmission range (0.45–11  $\mu\text{m}$ ), strong SHG responses (1.5 and 2.0 times that of commercial AGS) and high LIDTs (7 and 6 times that of AGS). Theoretical calculations revealed that the strong SHG effects of  $\text{Ca}_2\text{La}(\text{MS}_4)(\text{BS}_3)$  are contributed by the synergistic effects of  $\text{LaS}_6$ ,  $\text{MS}_4$  and  $\text{BS}_3$  groups. These results demonstrate that introducing more active functional groups in an excellent structure frame could be an effective method to achieve overall high IR NLO performances.

## Data availability

Supporting data for this article are presented in the ESI.† The raw data of this article can be obtained by contacting the corresponding author.

## Conflicts of interest

There are no conflicts to declare.

## Acknowledgements

The authors thank Dr Bing-Xuan Li (Fujian Institute of Research on Structure of Matter, Chinese Academy of Sciences) for his help with the LIDT test. This work was supported by the National Natural Science Foundation of China (No. 22031009, 22375201, and 21921001) and the Self-deployment Project Research Program of Haixi Institutes, Chinese Academy of Sciences (CXZX-2022-GH06).

## References

- 1 Y. Tang, K. Li, X. Zhang, J. Deng, G. Li and E. Brasselet, Harmonic spin-orbit angular momentum cascade in nonlinear optical crystals, *Nat. Photonics*, 2020, **14**, 658–662.
- 2 T. Verbiest, S. V. Elshocht, M. Kauranen, L. Hellemaans, J. Snauwaert, C. Nuckolls, T. J. Katz and A. Persoons, Strong enhancement of nonlinear optical properties through supramolecular chirality, *Science*, 1998, **282**, 913–915.
- 3 F. Capasso, R. Paiella, R. Martini, R. Colombelli, C. Gmachl, T. L. Myers, M. S. Taubman, R. M. Williams, C. G. Bethea, K. Unterrainer, H. Y. Hwang, D. L. Sivco, A. Y. Cho, A. M. Sergent, H. C. Liu and E. A. Whittaker, Quantum cascade lasers: ultrahigh-speed operation, optical wireless communication, narrow linewidth, and far-infrared emission, *IEEE J. Quantum Electron.*, 2002, **38**, 511–532.
- 4 D. F. Eaton, Nonlinear optical materials, *Science*, 1991, **253**, 281–287.
- 5 G. C. Catella, L. R. Shiozawa, J. R. Hietanen, R. C. Eckardt, R. K. Route, R. S. Feigelson, D. G. Cooper and C. L. Marquardt, Mid-IR absorption in AgGaSe<sub>2</sub> optical parametric oscillator crystals, *Appl. Opt.*, 1993, **32**, 3948–3951.
- 6 A. Harasaki and K. Kato, New Data on the nonlinear optical constant, phase-matching, and optical damage of AgGaS<sub>2</sub>, *Jpn. J. Appl. Phys.*, 1997, **36**, 700–703.
- 7 P. A. Budni, L. A. Pomeranz, M. L. Lemons, C. A. Miller, J. R. Mosto and E. P. Chicklis, Efficient mid-infrared laser using 1.9 μm-pumped Ho:YAG and ZnGeP<sub>2</sub> optical parametric oscillators, *J. Opt. Soc. Am. B*, 2000, **17**, 723–728.
- 8 K. Wu and S. Pan, A review on structure-performance relationship toward the optimal design of infrared nonlinear optical materials with balanced performances, *Coord. Chem. Rev.*, 2018, **377**, 191–208.
- 9 J. Chen, C. L. Hu, F. Kong and J. G. Mao, High-performance second-harmonic-generation (SHG) materials: new developments and new strategies, *Acc. Chem. Res.*, 2021, **54**, 2775–2783.
- 10 Y. Li, J. Luo and S. Zhao, Local polarity-induced assembly of second-order nonlinear optical materials, *Acc. Chem. Res.*, 2022, **55**, 3460–3469.
- 11 W. Wang, D. Mei, F. Liang, J. Zhao, Y. Wu and Z. Lin, Inherent laws between tetrahedral arrangement pattern and optical performance in tetrahedron-based mid-infrared nonlinear optical materials, *Coord. Chem. Rev.*, 2020, **421**, 213444.
- 12 H. Chen, M. Ran, W. Wei, X. Wu, H. Lin and Q. Zhu, A comprehensive review on metal chalcogenides with three-dimensional frameworks for infrared nonlinear optical applications, *Coord. Chem. Rev.*, 2022, **470**, 214706.
- 13 Y. Li, W. Wang, H. Wang, H. Lin and L. Wu, Mixed-anion inorganic compounds: a favourable candidate for infrared nonlinear optical materials, *Cryst. Growth Des.*, 2019, **19**, 4172–4192.
- 14 Y. Pan, S. Guo, B. Liu, H. Xue and G. Guo, Second-order nonlinear optical crystals with mixed anions, *Coord. Chem. Rev.*, 2018, **374**, 464–496.
- 15 W. Zhou and S.-P. Guo, Rational Design of Novel Promising Infrared Nonlinear Optical Materials: Structural Chemistry and Balanced Performances, *Acc. Chem. Res.*, 2024, **57**, 648–660.
- 16 X.-H. Li, Z.-H. Shi, M. Yang, W. Liu and S.-P. Guo, Sn<sub>7</sub>Br<sub>10</sub>S<sub>2</sub>: The First Ternary Halogen-Rich Chalcogenide Exhibiting a Chiral Structure and Pronounced Nonlinear Optical Properties, *Angew. Chem., Int. Ed.*, 2022, **61**, e202115871.
- 17 J. Chen, H. Chen, F. Xu, L. Cao, X. Jiang, S. Yang, Y. Sun, X. Zhao, C. Lin and N. Ye, Mg<sub>2</sub>In<sub>3</sub>Si<sub>2</sub>P<sub>7</sub>: A quaternary diamond-like phosphide infrared nonlinear optical material derived from ZnGeP<sub>2</sub>, *J. Am. Chem. Soc.*, 2021, **143**, 10309–10316.
- 18 Y. Chu, P. Wang, H. Zeng, S. Cheng, X. Su, Z. Yang, J. Li and S. Pan, Hg<sub>3</sub>P<sub>2</sub>S<sub>8</sub>: A new promising infrared nonlinear optical material with a large second-harmonic generation and a high laser-induced damage threshold, *Chem. Mater.*, 2021, **33**, 6514–6521.
- 19 G. Li, Y. Chu and Z. Zhou, From AgGaS<sub>2</sub> to Li<sub>2</sub>ZnSi<sub>4</sub>: realizing impressive high laser damage threshold together with large second-harmonic generation response, *Chem. Mater.*, 2018, **30**, 602–606.
- 20 M.-M. Chen, H.-G. Xue and S.-P. Guo, Multinary metal chalcogenides with tetrahedral structures for second-order nonlinear optical, photocatalytic, and photovoltaic applications, *Coord. Chem. Rev.*, 2018, **368**, 115–133.
- 21 X. Huang, S.-H. Yang, X.-H. Li, W. Liu and S. Guo, Eu<sub>2</sub>P<sub>2</sub>S<sub>6</sub>: The First Rare-Earth Chalcogenophosphate Exhibiting Large Second-Harmonic Generation Response and High Laser-Induced Damage Threshold, *Angew. Chem., Int. Ed.*, 2022, **61**, e202206791.
- 22 A. Abudurusuli, J. Huang, P. Wang, Z. Yang, S. Pan and J. Li, Li<sub>4</sub>MgGe<sub>2</sub>S<sub>7</sub>: the first alkali and alkaline-earth diamond-like infrared nonlinear optical material with exceptional large band gap, *Angew. Chem., Int. Ed.*, 2021, **60**, 24131–24136.
- 23 X. Lin, G. Zhang and N. Ye, Growth and characterization of BaGa<sub>4</sub>S<sub>7</sub>: a new crystal for mid-ir nonlinear optics, *Cryst. Growth Des.*, 2009, **9**, 1186–1189.
- 24 J. Yao, D. Mei, L. Bai, Z. Lin, W. Yin, P. Fu and Y. Wu, BaGa<sub>4</sub>Se<sub>7</sub>: a new congruent-melting ir nonlinear optical material, *Inorg. Chem.*, 2010, **49**, 9212–9216.
- 25 Q. Liu, X. Liu, L. Wu and L. Chen, SrZnGeS<sub>4</sub>: a dual-waveband nonlinear optical material with a transparency spanning uv/vis and far-ir spectral regions, *Angew. Chem., Int. Ed.*, 2022, **61**, e202205587.
- 26 Y. Guo, F. Liang, W. Yin, Z. Li, X. Luo, Z.-S. Lin, J. Yao, A. Mar and Y. Wu, BaHgGeSe<sub>4</sub> and SrHgGeSe<sub>4</sub>: Two new hg-based infrared nonlinear optical materials, *Chem. Mater.*, 2019, **31**, 3034–3040.
- 27 B.-W. Liu, X.-M. Jiang, H.-Y. Zeng and G.-C. Guo, [ABa<sub>2</sub>Cl][Ga<sub>4</sub>S<sub>8</sub>] (A = Rb, Cs): wide-spectrum nonlinear

- optical materials obtained by polycation-substitution-induced nonlinear optical (nlo)-functional motif ordering, *J. Am. Chem. Soc.*, 2020, **142**, 10641–10645.
- 28 Z.-X. Wu, W.-F. Chen, X.-M. Jiang, B.-W. Liu and G.-C. Guo, [Na<sub>2</sub>PbI][Ga<sub>7</sub>S<sub>12</sub>]: combining diamond-like anionic framework with polycationic chain toward achieving remarkable nonlinear optical response, *Chem. Mater.*, 2024, **36**, 3444–3451.
- 29 G. A. Marking, J. A. Hanko and M. G. Kanatzidis, New quaternary thioannates and thiogermanates A<sub>2</sub>Hg<sub>3</sub>M<sub>2</sub>S<sub>8</sub> (A = Cs, Rb; M = Sn, Ge) through Molten A<sub>2</sub>S<sub>x</sub> reversible glass formation in Cs<sub>2</sub>Hg<sub>3</sub>M<sub>2</sub>S<sub>8</sub>, *Chem. Mater.*, 1998, **10**, 1191–1199.
- 30 C. Li, W. Yin, P. Gong, X. Li, M. Zhou, A. Mar, Z. Lin, J. Yao, Y. Wu and C. Chen, Trigonal planar [HgSe<sub>3</sub>]<sup>4-</sup> unit: a new kind of basic functional group in ir nonlinear optical materials with large susceptibility and physicochemical stability, *J. Am. Chem. Soc.*, 2016, **138**, 6135–6138.
- 31 L. Luo, L. A. Wang, J. B. Chen, J. Z. Zhou, Z. H. Yang, S. L. Pan and J. J. Li, AIB<sub>3</sub>IIC<sub>3</sub>IIIQ<sub>8</sub>VI: a new family for the design of infrared nonlinear optical materials by coupling octahedra and tetrahedra units, *J. Am. Chem. Soc.*, 2022, **144**, 21916–21925.
- 32 H. Li, G. Li, K. Wu, B. Zhang, Z. Yang and S. Pan, BaB<sub>2</sub>S<sub>4</sub>: an efficient and air-stable thioborate as infrared nonlinear optical material with high laser damage threshold, *Chem. Mater.*, 2018, **30**, 7428–7432.
- 33 Y.-X. Han, C.-L. Hu, Z. Fang, Q.-Q. Chen, B.-X. Li, Y. Lin and J.-G. Mao, LaBS<sub>3</sub> revisited: a promising mid-infrared nonlinear optical material, *J. Mater. Chem. C*, 2022, **10**, 12556–12559.
- 34 J. Zhou, K. Hou, Y. Chu, Z. Yang, J. Li and S. Pan, AIB<sub>3</sub>IIC<sub>2</sub>IIIQ<sub>6</sub>VIXVII: A Thioborate Halide Family for Developing Wide Bandgap Infrared Nonlinear Materials by Coupling Planar [BS<sub>3</sub>] and Polycations, *Small*, 2024, **20**, 2308806.
- 35 Y.-Y. Li, B.-X. Li, G. Zhang, L.-J. Zhou, H. Lin, J.-N. Shen, C.-Y. Zhang, L. Chen and L.-M. Wu, Syntheses, characterization, and optical properties of centrosymmetric Ba<sub>3</sub>(BS<sub>3</sub>)<sub>1.5</sub>(MS<sub>3</sub>)<sub>0.5</sub> and noncentrosymmetric Ba<sub>3</sub>(BQ<sub>3</sub>)(SbQ<sub>3</sub>), *Inorg. Chem.*, 2015, **54**, 4761–4767.
- 36 Y. Lian, L.-M. Wu and L. Chen, Thioborates: potential nonlinear optical materials with rich structural chemistry, *Dalton Trans.*, 2017, **46**, 4134–4147.
- 37 Y. Han, C. Hu and J. Mao, Ca<sub>2</sub>Ln(BS<sub>3</sub>)(Si<sub>4</sub>) (Ln = La, Ce, and Gd): Mixed Metal Thioborate–Thiosilicates as Well-Performed Infrared Nonlinear Optical Materials, *Small*, 2024, **20**, 2305828.
- 38 A. K. Iyer, J. B. Cho, H. R. Byun, M. J. Waters, S. Hao, B. M. Oxley, V. Gopalan, C. Wolverton, J. M. Rondinelli, J. I. Jang and M. G. Kanatzidis, Structure tuning, strong second harmonic generation response, and high optical stability of the polar semiconductors Na<sub>1-x</sub>K<sub>x</sub>AsQ<sub>2</sub>, *J. Am. Chem. Soc.*, 2021, **143**, 18204–18215.
- 39 Y. Pi, Y. Kuk and K. M. Ok, Small changes, big impact: tungsten bronzes with extremely large second harmonic generation achieved by the transition metal doping on the b-site, *Adv. Funct. Mater.*, 2023, **33**, 2214985.
- 40 Y. Kuk, S. B. Bae, S. M. Yang and K. M. Ok, A Polar Tetragonal Tungsten Bronze with Colossal Second-Harmonic Generation, *Adv. Sci.*, 2023, **10**, 2301374.
- 41 P. Wang, Y. Chu, A. Tudi, C. Xie, Z. Yang, S. Pan and J. Li, The combination of structure prediction and experiment for the exploration of alkali-earth metal-contained chalcopyrite-like ir nonlinear optical material, *Adv. Sci.*, 2022, **9**, 2106120.
- 42 Z. Li, S. Zhang, Z. Huang, L.-D. Zhao, E. Uykur, W. Xing, Z. Lin, J. Yao and Y. Wu, Molecular construction from AgGaS<sub>2</sub> to CuZnPS<sub>4</sub>: defect-induced second harmonic generation enhancement and cosubstitution-driven band gap enlargement, *Chem. Mater.*, 2020, **32**, 3288–3296.
- 43 R. Li, Q. Liu, X. Liu, Y. Liu, X. Jiang, Z. Lin, F. Jia, L. Xiong, L. Chen and L. Wu, Na<sub>2</sub>Ba[Na<sub>2</sub>Sn<sub>2</sub>S<sub>7</sub>]: Structural Tolerance Factor-Guided NLO Performance Improvement, *Angew. Chem., Int. Ed.*, 2023, **62**, e202218048.
- 44 W. Zhou, M. Geng, M. Yan, N.-T. Suen, W. Liu and S.-P. Guo, Alkali metal partial substitution-induced improved second-harmonic generation and enhanced laser-induced damage threshold for Ag-based sulfides, *Inorg. Chem. Front.*, 2022, **9**, 3779–3787.
- 45 J. Kuchinke, A. Hammerschmidt and B. Krebs, Rb<sub>8</sub>[B<sub>12</sub>(BS<sub>3</sub>)<sub>6</sub>] and Cs<sub>8</sub>[B<sub>12</sub>(BS<sub>3</sub>)<sub>6</sub>]: the first thioborato-closo-dodecaborates, *Solid State Sci.*, 2003, **5**, 189–196.
- 46 S.-P. Guo, G.-C. Guo, M.-S. Wang, J.-P. Zou, H.-Y. Zeng, L.-Z. Cai and J.-S. Huang, A facile approach to hexanary chalcogenoborate featuring a 3-D chiral honeycomb-like open-framework constructed from rare-earth consolidating thiogallate-closo-dodecaborate, *Chem. Commun.*, 2009, 4366–4368.
- 47 S.-P. Guo, G.-C. Guo, M.-S. Wang, J.-P. Zou, G. Xu, G.-J. Wang, X.-F. Long and J.-S. Huang, A Series of New Infrared NLO Semiconductors, ZnY<sub>6</sub>Si<sub>2</sub>S<sub>14</sub>, Al<sub>x</sub>Dy<sub>3</sub>(Si<sub>y</sub>Al<sub>1-y</sub>)S<sub>7</sub>, and Al<sub>0.33</sub>Sm<sub>3</sub>Si<sub>7</sub>, *Inorg. Chem.*, 2009, **48**, 7059–7065.
- 48 J. Wang, Y. Cheng, H. Wu, Z. Hu, J. Wang, Y. Wu and H. Yu, Sr<sub>3</sub>[SnOSe<sub>3</sub>][CO<sub>3</sub>]: a heteroanionic nonlinear optical material containing planar π-conjugated [CO<sub>3</sub>] and heteroleptic [SnOSe<sub>3</sub>] anionic groups, *Angew. Chem., Int. Ed.*, 2022, **61**, e202201616.
- 49 K. Wu, Z. Yang and S. Pan, Na<sub>2</sub>Hg<sub>3</sub>M<sub>2</sub>S<sub>8</sub> (M = Si, Ge, and Sn): new infrared nonlinear optical materials with strong second harmonic generation effects and high laser-damage thresholds, *Chem. Mater.*, 2016, **28**, 2795–2801.
- 50 Y. Yang, Y. Chu, B. Zhang, K. Wu and S. Pan, Unique Unilateral-Chelated Mode-Induced d-p-π Interaction Enhances Second-Harmonic Generation Response in New Ln<sub>3</sub>LiMS<sub>7</sub> Family, *Chem. Mater.*, 2021, **33**, 4225–4230.
- 51 B. Krebs and W. Hamann, Ortho-thioborates and ortho-selenoborates: synthesis, structure and properties of Tl<sub>3</sub>BS<sub>3</sub> and Tl<sub>3</sub>BSe<sub>3</sub>, *J. Less-Common Met.*, 1988, **137**, 143–154.
- 52 M. J. Frisch, G. W. Trucks, H. B. Schlegel, G. E. Scuseria, M. A. Robb, J. R. Cheeseman, G. Scalmani, V. Barone,

- B. Mennucci, G. A. Petersson, H. Nakatsuji, M. Caricato, X. Li, H. P. Hratchian, A. F. Izmaylov, J. Bloino, G. Zheng, J. L. Sonnenberg, M. Hada, M. Ehara, K. Toyota, R. Fukuda, J. Hasegawa, M. Ishida, T. Nakajima, Y. Honda, O. Kitao, H. Nakai, T. Vreven, J. A. Montgomery Jr, J. E. Peralta, F. Ogliaro, M. Bearpark, J. J. Heyd, E. Brothers, K. N. Kudin, V. N. Staroverov, R. Kobayashi, J. Normand, K. Rendell, A. Raghavachari, J. C. Burant, S. S. Iyengar, J. Tomasi, M. Cossi, N. Rega, J. M. Millam, M. Klene, J. E. Knox, J. B. Cross, V. Bakken, C. Adamo, J. Jaramillo, R. Gomperts, R. E. Stratmann, O. Yazyev, A. J. Austin, R. Cammi, C. Pomelli, J. W. Ochterski, R. L. Martin, K. Morokuma, V. G. Zakrzewski, G. A. Voth, P. Salvador, J. J. Dannenberg, S. Dapprich, A. D. Daniels, O. Farkas, J. B. Foresman, J. V. Ortiz, J. Cioslowski and D. J. Fox, *Gaussian 09, revision A.07*, Gaussian, Inc., Wallingford, CT, 2009.
- 53 Y. Yun, M. Wu, C. Xie, Z. Yang, G. Li and S. Pan, Theoretical prediction-assisted synthesis and characterization of infrared nonlinear optical material NaSrBS<sub>3</sub>, *Adv. Opt. Mater.*, 2023, **11**, 2300256.
- 54 V. Milman, B. Winkler, J. A. White, C. J. Pickard, M. C. Payne, E. V. Akhmatkaya and R. H. Nobes, Electronic structure, properties, and phase stability of inorganic crystals: A pseudopotential plane-wave study, *Int. J. Quantum Chem.*, 2000, **77**, 895–910.
- 55 M. D. Segall, P. J. D. Lindan, M. J. Probert, C. J. Pickard, P. J. Hasnip, S. J. Clark and M. C. Payne, First-principles simulation: ideas, illustrations and the CASTEP code, *J. Phys.: Condens. Matter*, 2002, **14**, 2717–2744.